Glancing angle Talbot-Lau grating interferometers for phase contrast imaging at high x-ray energy

D. Stutman and M. Finkenthal

Department of Physics and Astronomy, Johns Hopkins University, Baltimore, Maryland 21218, USA

A Talbot-Lau interferometer is demonstrated using micro-periodic gratings inclined at a glancing angle along the light propagation direction. Due to the increase in the effective thickness of the absorption gratings, the device enables differential phase contrast imaging at high x-ray energy, with improved fringe visibility (contrast). For instance, at 28° glancing angle, we obtain up to ~35% overall interferometer contrast with a spectrum having ~43 keV mean energy, suitable for medical applications. In addition, glancing angle interferometers could provide high contrast at energies above 100 keV, enabling industrial and security applications of phase contrast imaging. © 2012 American Institute of Physics. [http://dx.doi.org/10.1063/1.4748882]

Differential phase-contrast (DPC) or refraction based x-ray imaging with Talbot-Lau grating interferometers is a technique investigated for its capability to image low-Z mater with improved contrast.[1,2] Possible applications range from biomedical, to material sciences, to non-destructive testing (NDT), and to energy research.[1–6] As an example of medical application, Talbot-Lau interferometry is studied for phase-contrast imaging of joint soft tissues, towards an improved diagnostic of rheumatoid arthritis and osteoarthritis disease.[5]

The conventional Talbot-Lau interferometer consists of three micro-periodic gratings at normal incidence ("source," "beam-splitter," and "analyzer"), which make an extended area angular filter having a few μ-radian resolution.[1,2] By blocking or transmitting the x-rays according to their propagation direction, this filter converts into intensity changes on a conventional detector the small angular deviations due to x-ray refraction in the imaged object. The beam-splitter is usually a thin phase grating, while the source and analyzer are thick absorption gratings made by filling with Au the gaps in a Si or a photoresist substrate. Typical grating periods are in the 3-10 μm range. The attractiveness of the Talbot-Lau method for practical applications is that it can work with extended area and spectrally broad x-ray sources, such as the high power W anode tubes used for medical imaging.[1–3]

A practical limitation of the Talbot-Lau grating interferometer is that, due to the limited absorber thickness possible for few-micron period gratings, the fringe visibility or contrast is decreasing rapidly with x-ray energy. The absorber thickness is limited by the technologically feasible grating aspect-ratio (thickness/period), which is at present around 20–25.[7] Thus, for instance, the bars of an Au grating of 100 μm thickness will absorb only ~58% of 60 keV x-rays; ~350 μm Au thickness would be needed for 95% absorption. The effect on the interferometer contrast is illustrated in Fig. 1 with the computed contrast for first Talbot order (m = 1) interferometers, having 100 μm thick Au gratings at normal incidence and "design" or mean energies of 30 keV and of 60 keV. All the gratings have 10 μm period; the beam-splitter was assumed to be a π-shift Si phase having thickness of 39 μm at 30 keV and of 78 μm at 60 keV. The overall interferometer contrast is

computed as $V \equiv (I_{BF} - I_{DF})/(I_{BF} + I_{DF})$, with I_{BF} and I_{DF} the "bright-field" and the "dark-field" intensity, respectively.[1,2] The computation was done with a model based on the XWFP (X-ray Wave Front Propagation) wave propagation code,[8] which includes the contrast decrease due to the width of the source grating openings. An opening of 1/2 the period, i.e., a duty-cycle of 50%, was used for all the gratings. Assuming perfectly absorbing source and analyzer gratings, the maximal computed contrast is ~36%.

As seen in Fig. 1, the 100 μm Au gratings enable achieving close to maximal contrast only in the 30 keV case; in the 60 keV case, the peak contrast reaches only ~8% and occurs at considerably lower energy than the design energy. In addition, for an interferometer working with a spectrally broad x-ray tube, the effective contrast is further reduced by spectral averaging.[9,10]

At the same time, numerical simulations indicate that high (>20%) interferometer contrast is critical for high energy applications of the Talbot-Lau method.[10,11] For instance, in Ref. 11, it is computed that the noise in the phase gradient image would decrease by more than an order of magnitude if the interferometer contrast would increase from 10% to 50%.
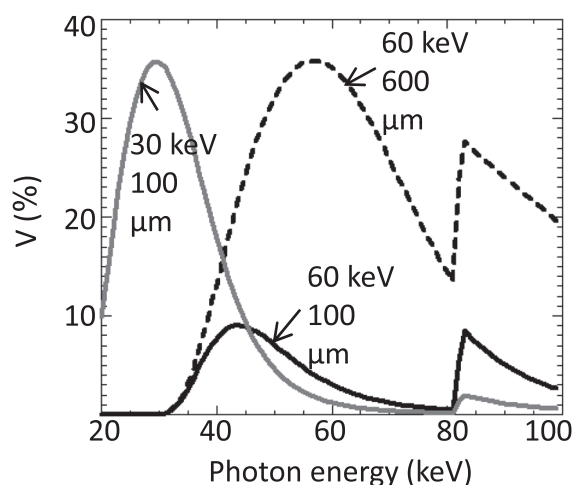

FIG. 1. Computed contrast for m = 1 normal incidence Talbot-Lau interferometers assuming 100 μm thick Au source and 30 or 60 keV design energy. Also shown is the 60 keV case assuming 600 μm thick Au gratings.
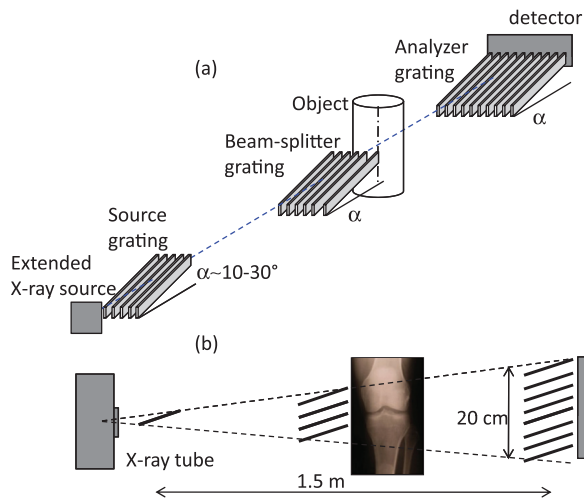
FIG. 2. (a) Layout of the glancing angle Talbot-Lau grating interferometer. (b) Method for achieving large field of view using multiple stacked gratings at glancing angle.

This happens because the contrast together with the angular resolution determines the sensitivity $\Delta I/\Delta\theta$ with which the interferometer converts angular x-ray deviations $\Delta\theta$ into intensity changes ΔI. In addition, high contrast is important at high x-ray energy because the refraction angles decrease rapidly with energy (approximately as $1/E^2$ (Ref. 3)).

Our paper demonstrates a type of Talbot-Lau grating interferometer that enables achieving high contrast at high x-ray energy, using relatively thin gratings that can be easily produced with the existent technology. The proposed design uses gratings inclined at a glancing angle $\alpha \sim 10° - 30°$ with respect to the axis of the x-ray beam, with the grating bars oriented *along* the direction of the beam (Fig. 2(a)). In this way, the x-ray path through the absorption gratings increases from the normal incidence value t, to a value of $t/\sin(\alpha)$. This in turn can strongly increase the interferometer contrast, as illustrated in Fig. 1 with the computed contrast for a 60 keV interferometer having 600 μm thick Au gratings, as would be obtained using for instance 100 μm thick gratings at $\sim 10°$ glancing incidence. A similar design was earlier proposed by us using "physical period" mirror gratings at grazing incidence.[12]

Inclining the gratings increases also the x-ray path through the phase grating, so that for a given design energy, its thickness can be decreased from the normal incidence value by a factor of $\sin(\alpha)$. At the same time, the increase in the x-ray path through the thin grating substrates does not lead to strong beam attenuation. For instance, 60 keV photons passing through three 150 μm thick Si substrates at 10° glancing angle would be attenuated by only $\sim 8\%$.

The practical limitation in the design in Fig. 2(a) is that the field of view in the grating inclination direction is reduced by a factor of $\sin(\alpha)$. For typical grating sizes of 7-10 cm, this constrains the field of view in the inclination direction to ~ 1-5 cm at 10°-30° glancing angles. Large field of view could however be simply obtained by stacking several gratings as in Fig. 2(b).

Another constraint, shared with the normal incidence Talbot-Lau interferometer, is that the field of view in the direction orthogonal to the grating bars (horizontal in Fig. 2(a)) is limited (vignetted) by the analyzer, which acts as a

collimator with small opening to length ratio. At glancing incidence, this effect is enhanced by the larger effective collimation length.

While the design in Fig. 2(a) appears as a straightforward modification of the normal incidence Talbot-Lau interferometer, we note that it is difficult to theoretically assess whether such a configuration will work with an extended x-ray source and in cone beam geometry. Oblique incidence Talbot-Lau interferometers having the grating bars *perpendicular* to the direction of the x-ray beam have been proposed in Ref. 12 and analytically and experimentally studied in Ref. 13. The analysis in Ref. 13 was based on the approximation that the grating transmission function depends only on the coordinates in the grating principal planes and not on the coordinate along the beam direction. Thus, the effect of inclining the gratings is simply to increase the apparent or effective period, by a factor of $1/\sin(\alpha)$. This assumption is no longer possible however in the case of gratings with the bars oriented *along* the x-ray beam as in Fig. 2.

We therefore used an experimental approach to investigate whether glancing incidence Talbot-Lau interferometers can work with conventional x-ray tubes in cone beam geometry and whether they increase the contrast at high energy. For the experiments, we used a 5.4 μm period "symmetric" interferometer, in which the grating periods and the inter-grating distances are equal. The symmetric configuration provides maximal angular sensitivity for a given interferometer length.[5] The glancing angle was varied in the range $\sim 15°$-45°. The source and analyzer gratings had 90 μm thick Au bars, while the phase grating had 7 μm thick Ni bars. As design or mean operating energy, we chose 43 keV, which is approximately the mean energy of the transmitted spectrum in the conventional x-ray radiography of the knee, typically done with W anode tubes at 60 kVp. Assuming that the phase shift of the inclined phase grating is determined by the effective thickness $t/\sin(\alpha)$, the Ni grating would produce a π phase shift for 43 keV x-rays when inclined at 28°. To compare the glancing incidence and the normal incidence interferometers, we used also an Au phase grating with 8.5 μm thick bars, computed to produce a π phase shift for 43 keV
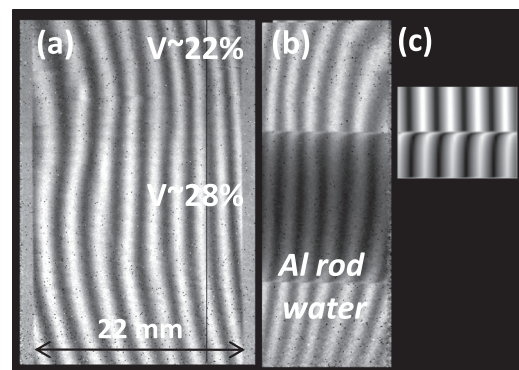

FIG. 3. (a) Moiré fringe pattern obtained with m = 3 interferometer using gratings inclined at 28°. The pattern size is 22 × 37 mm at the analyzer location. The gratings were inclined in the horizontal plane instead of vertical as in Fig. 2(a). Also shown is the central and peripheral fringe contrast. The vertical intensity variation due to analyzer vignetting was removed by normalizing an image without the grating. (b) Moiré fringe pattern from 9 mm Al rod immersed in 100 mm water layer, using the m = 3 interferometer at 18° glancing angle. (c) XWFP simulation of the Al rod immersed in water.

x-rays at normal incidence. All the gratings had 50% duty-cycle and were made by MicroWorks, Inc., Germany.

The detector was a 38×38 mm, $150\,\mu$m thick CsI scintillator optically coupled to a cooled CCD. The interferometer was operated in the m = 1 and m = 3 Talbot orders, with a total length of 0.52 and 1.56 m, respectively. Operation in higher Talbot orders is needed to achieve sufficient angular resolution for soft tissue applications.[5] To produce a spectrum with ~43 keV mean energy, we used a W anode tube operated at 60 kVp/1 mA and filtered the radiation through a 100 mm thick water tank. The samples to be imaged were placed in the tank at a distance R ~ 6 cm behind the center of the beam-splitter grating. This decreases the sensitivity to refraction at the sample by a factor 1-R/D, with D the beam-splitter to analyzer distance.[5,9] For the m = 3 interferometer, the decrease is only ~7%. This setup was used in all the experiments below, with typical integration times of 30 s for $80 \times 80\,\mu$m detector pixels.

The experimental results are illustrated in Figs. 3–5. Fig. 3(a) shows a 22×37 mm moiré fringe pattern obtained with the interferometer in the m = 3 Talbot order and with all the gratings inclined at 28° glancing angle (effective Au thickness ~190 μm). The moiré fringes were produced by rotating the analyzer with respect to the Talbot pattern. The fringe contrast $V = (I_{max} - I_{min})/(I_{max} + I_{min})$ reaches the remarkably high value of ~28% in the central region, decreasing to ~22% at the periphery. (Note that the contrast of a large period moiré pattern is essentially equal to the "dark field/bright field" contrast above defined.) The pattern is slightly distorted due to imperfections in the gratings and alignment, amplified also by the glancing incidence. Nevertheless, the result in Fig. 3 clearly demonstrates that glancing angle grating interferometers can work and also provide high fringe contrast at high energy.

To verify that the glancing angle setup simultaneously provides both high interferometer contrast and high angular resolution, we measured the moiré fringe shift produced by a 9 mm diameter Al rod immersed in the 100 mm water tank. This combination is computed with the XWFP code to produce a ~2 μrad refraction angle at the rod edges for 43 keV x-rays. (Since the refraction angle diverges at the very edge of the rod, we use as representative value the angle at ~0.1 mm inside the rod diameter, i.e., at a radius of ~4.4 mm.) The rod was imaged using the m = 3 interferometer with the gratings inclined at 18° (effective Au thickness ~290 μm). The 7 μm Ni phase grating was used as beam-splitter. At this inclination, the grating is computed to produce a ~1.4 π phase shift for photons of 43 keV. The theoretical angular resolution, given by the ratio between the analyzer period and the Talbot distance, is ~6.9 μrad. Moiré fringe shifts of ~1/3 the fringe period are thus expected in this setup, as also shown by the XWFP simulation in Fig. 3(c). The experimental fringe pattern and shift in Fig. 3(b) match indeed the XWFP calculation, confirming that the interferometer functions with the expected angular resolution.

Due to analyzer vignetting, the photon count decreases from the center to the top and to the bottom of the image in Fig. 3(a). At 28° glancing angle, the rate of intensity decrease is around 13%/cm. Interestingly, however, the interferometer contrast decreases at a considerably lower rate, of only ~3.5%/cm. At 18° glancing angle, the rate of intensity decrease about doubles, consistent with doubled effective aspect-ratio of the analyzer, while the rate of contrast loss is ~5%/cm. This is also an encouraging result; due to the high contrast values achieved with the glancing angle interferometer in the center of the image, a 5%-10% contrast decrease towards the edges of the image becomes tolerable. The contrast decrease from the center to the periphery of the image in cone-beam geometry can be explained by the deviation from rectangular shape of the beam-splitter and analyzer grating bars, when viewed at an angle away from normal.[14]

The strong contrast increase possible with the glancing angle interferometer is illustrated in Figs. 4(a)–4(c), which compare the moiré fringe contrast obtained with first and third order interferometers, at grating angles ranging from normal incidence to 18°. The moiré pattern images have the same contrast scale. The central fringe contrast V obtained from the fringe intensity variation is also shown in each figure.

The contrast obtained with the normal incidence interferometer at high energy is modest, even when using high aspect-ratio gratings: around 13% in the first Talbot order and 9% in the third order. The contrast however nearly triples in both orders when using the 28° glancing angle interferometer. The simultaneous achievement of high contrast and high angular resolution in the third Talbot order is promising for medical applications. Also encouraging for extrapolation to higher x-ray energy is that this trend continues at
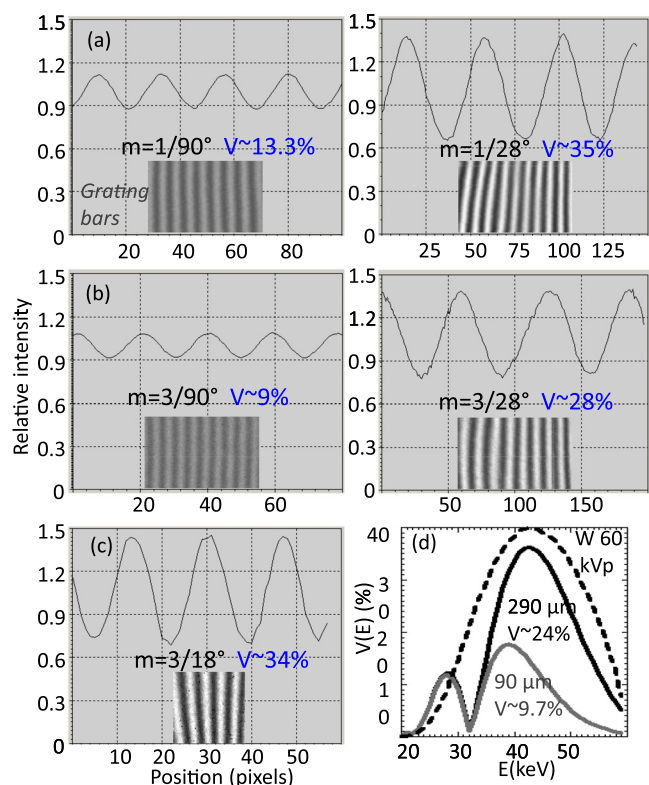

FIG. 4. (a) Moiré fringe pattern and intensity profile for m = 1, $\langle E \rangle \sim 43$ keV interferometer at 90° and at 28° glancing angle. (b) and (c) Similar result for m = 3 interferometer at 90°, 28°, and 18° glancing angles. (d) Computed contrast for m = 3, $\langle E \rangle = 43$ keV interferometer using 90 μm and 290 μm thick Au gratings; also shown is the computed spectrum of a 60 kVp W anode tube filtered with 100 mm water.
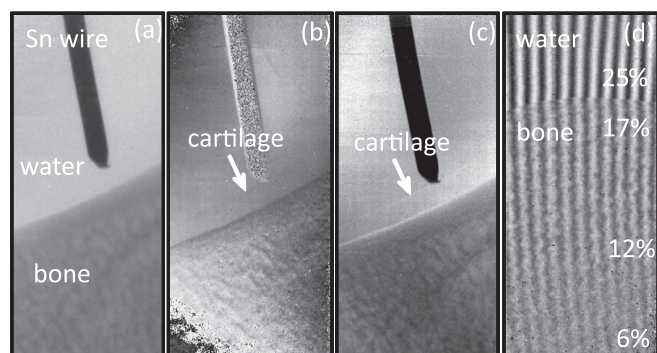
FIG. 5. Attenuation (a), phase gradient (b), and refraction enhanced image (c) of fresh lamb hip bone in 100 mm water tank, obtained with m = 3 interferometer at 28° grating angle. (d) Moiré fringe image of the same bone; also shown is the fringe visibility decrease as the thickness of the bone traversed by the x-rays increases.

smaller inclination angles, with ∼34% contrast achieved in the third order using gratings inclined at 18°.

While the experiment shows that the glancing angle interferometer can strongly improve contrast at high energy, it is not clear however whether this improvement can be attributed only to the increased effective absorber thickness. To evaluate the contrast increase expected from the increased effective absorption length at glancing incidence, we used normal incidence calculations with our XWFP based model, in which we varied the Au thickness in the source and analyzer gratings. Fig. 4(d) shows the predicted spectral dependence of the m = 3 contrast for 90 μm Au thickness (corresponding to the normal incidence gratings) and for 290 μm thickness (gratings inclined at 18°). For comparison with experiment, the contrast was averaged over the spectrum of the 60 kVp W anode tube, filtered with 100 mm water absorber. The spectral dependence of the detector efficiency was taken as proportional to the fraction of absorbed x-rays in the CsI scintillator and to the photon energy. As seen, the 9.7% computed contrast at normal incidence is close to the ∼9% experimental value in Fig. 3(b). The same good agreement holds for the m = 1 case; the computed contrast is 13.7% and the measured one 13.4%, indicating that our normal incidence interferometer model is quite accurate.

At glancing angles, however, the agreement between calculation and experiment breaks down. The m = 3 spectrally averaged contrast computed using the effective Au thickness corresponding to 18° inclination is only ∼24%, while the experimental value is ∼34%. For the effective Au thickness corresponding to 28° inclination, the computed contrast is 24.5% for m = 1 and 18.6% for m = 3, while the experimental values are 35% and 28%, respectively.

A possible explanation for this discrepancy is that, due to imperfect alignment of the gratings, the source grating openings viewed by the beam-splitter are slightly narrowed, thus increasing the coherence of the beam. As discussed in Ref. 8, this can have a strong effect on contrast, which is expected to vary as ∼exp$(-1.9 \, s/g)^2$, with s the source grating opening and g the period. In addition, any angular misalignment between the gratings in the direction perpendicular to the inclination plane is amplified by the glancing incidence. The existence of a small angular misalignment is suggested also by the observation of a somewhat larger than expected

intensity decrease when going from normal incidence to glancing incidence. For instance, with the m = 1 interferometer, we observe a 45% detector count decrease when going from 90° to 28°, while the expected decrease due to the increased absorption in the source and analyzer gratings is estimated at only ∼30%.

Nevertheless, the possibility exists also that the glancing angle Talbot-Lau interferometer functions somewhat differently from the normal incidence one. For instance, Braig et al. recently showed that EUV beam-splitter gratings operated at grazing incidence along the grating bars have better performance in comparison to gratings operated in the conventional manner, i.e., with the light perpendicular to the grating bars.[15]

Regardless of the exact mechanism for contrast increase, however, the high contrast attainable with glancing angle interferometers at high x-ray energy improves the practical applicability of Talbot-Lau interferometry. The potential for improved soft tissue imaging is illustrated in Fig. 5, which shows the conventional attenuation, the phase gradient, and the refraction enhanced images of a ∼35 mm diameter fresh lamb hip bone, immersed in the 100 mm water tank. The images were obtained with the m = 3 interferometer at 28° glancing angle and with the energetic spectrum in Fig. 4(d). The phase gradient image was obtained using a 16 exposure phase-scan, i.e., a scan of the relative position of the gratings.[1,2] The refraction enhanced image was obtained in a single exposure, with the interferometer tuned at the point of maximal sensitivity to angular changes.[5,16] As seen, while the thin cartilage layer is almost invisible in the attenuation image, it becomes apparent in the phase gradient image. More importantly, the simultaneous achievement of high contrast and angular sensitivity with the m = 3 glancing angle interferometer allows visualizing the cartilage also using a single exposure, refraction enhanced image. This opens the possibility for clinical phase-contrast enhanced imaging of soft tissues with reduced dose.

Further on, Fig. 5(d) shows a moiré image of the lamb hip bone obtained in the m = 3, 18° glancing angle setup. The notable feature is that due to the energetic x-ray spectrum and the high contrast of the glancing angle interferometer, the moiré fringes are still visible even after the x-rays traverse a few cm of bone. The fringe contrast variation is also indicated in Fig. 5(d), showing how the contrast progressively decreases due to the strong ultra-small angle scattering (USAXS) characteristic of bone.[17] High energy glancing angle interferometers could thus enable bone diagnostics, such as, for instance, USAXS based assessment of osteoporosis.

Finally, our calculations indicate that using glancing angle interferometers high contrast can be achieved also at x-ray energies above the Au K-edge at 80 keV, where the Au absorption strongly increases. We compute, for instance, that up to ∼40% contrast may be possible at ⟨E⟩ ∼ 110 keV using 100 μm thick, 40% duty-cycle Au gratings at 7° inclination. Such performance would open possibilities for industrial, NDT, and security applications of Talbot-Lau interferometers.

[1]F. Pfeiffer, T. Weitkamp, O. Bunk, and C. David, Nat. Phys. **2**, 258 (2006).

[2]A. Momose, W. Yashiro, Y. Takeda, Y. Suzuki, and T. Hattori, Jpn. J. Appl. Phys., Part 1 **45**, 5254 (2006).

[3]See, e.g., S. A. Zhou and A. Brahme, Phys. Medica **24**, 129 (2008) and references therein.

[4]V. Revol, I. Jerjen, C. Kottler, P. Schutz, R. Kaufmann, T. Luthi, U. Sennhauser, U. Straumann, and C. Urban, J. Appl. Phys. **110**, 044912 (2011).

[5]D. Stutman, T. Beck, J. Carrino, and C. Bingham, Phys. Med. Biol. **56**, 5697 (2011).

[6]D. Stutman and M. Finkenthal, Rev. Sci. Instrum. **82**, 113508 (2011).

[7]T. Weber, F. Bayer, W. Haas, G. Pelzer, J. Rieger, A. Ritter, L. Wucherer, J. Durst, T. Michel, and G. Anton, J. Instrum. **7**(2), P02003 (2012).

[8]T. Weitkamp, "Advances in computational methods for x-ray and neutron optics," Proc. SPIE **5536**, 181 (2004).

[9]M. Engelhard, C. Kottler, O. Bunk, C. David, C. Schroer, J. Baumann, M. Schuster, and F. Pfeiffer, J. Microsc. **232**, 145 (2008).

[10]V. Revol, C. Kottler, R. Kaufmann, U. Straumann, and C. Urban, Rev. Sci. Instrum. **81**, 073709 (2010).

[11]R. Raupach and T. G. Flohr, Phys. Med. Biol. **56**, 2219 (2011).

[12]D. Stutman, M. Finkenthal, and N. Moldovan, Appl. Opt. **49**, 4677 (2010).

[13]H. Wen, C. K. Kemble, and E. E. Bennett, Opt. Express **19**, 25093 (2011).

[14]V. Revol, C. Kottler, R. Kaufmann, I. Jerjen, T. Luthi, F. Cardot, P. Niedermann, U. Straumann, U. Sennhauser, and C. Urban, Nucl. Instrum. Methods Phys. Res. A **648**, S302 (2011).

[15]C. Braig, L. Fritzsch, T. Kasebier, E.-B. Kley, C. Laubis, Y. Liu, F. Scholze, and A. Tunnermann, Opt. Express **20**, 1825 (2012).

[16]P. Zhu, K. Zhang, Z. Wang, *et al*., Proc. Natl. Acad. Sci. U.S.A. **107**, 13576 (2010).

[17]M. De Felici, R. Felici, C. Ferrer, A. Bravin, A. Tartari, and M. Gambaccini, Nucl. Instrum. Methods Phys. Res. A **580**, 489 (2007).